J Solid State Electrochem (2012) 16:197–204
DOI 10.1007/s10008-011-1309-8

ORIGINAL PAPER

Growth and characterization of ZnO nanowire arrays electrodeposited into anodic alumina templates in DMSO solution

Humberto Gomez · Gonzalo Riveros · Daniel Ramirez · Rodrigo Henriquez · Ricardo Schrebler · Ricardo Marotti · Enrique Dalchiele

Received: 22 October 2010 / Revised: 4 January 2011 / Accepted: 12 January 2011 / Published online: 2 February 2011

Abstract ZnO nanowire arrays were grown by potentiostatic cathodic electrodeposition on aluminum anodic oxide template (AAO) from dimethyl sulfoxide (DMSO) solutions containing zinc chloride and molecular oxygen as precursors. The nanowires presented high aspect ratio and exhibited a very high crystallinity with a wurtzite crystal structure with preferential orientation along the (0001) crystallographic axis. Chronoamperometric experiments were performed on gold bulk electrodes in order to model this preferential mode growth of ZnO nanowires, which has not been previously reported for similar precursors in DMSO solution. The analysis of the corresponding chronoamperograms revealed that chloride ions influence the oxide nucleation and growth mechanism. It was found that in the absence of KCl as a supporting electrolyte, the data fitted an instantaneous three-dimensional diffusion-controlled $(IN\text{-}3D)_{diff}$ nucleation and growth mechanism (NGM). The presence of KCl, instead favored a progressive three-dimensional $(PN\text{-}3D)_{diff}$ NGM. With these results, a model for the more complex nanowire's growth inside the pores of the AAO template is proposed.

Keywords Zinc oxide · Nanowires · Electrodeposition · AAO template · Nucleation and growth mechanism

G. Riveros · D. Ramirez
Departamento de Química y Bioquímica, Instituto de Física,
Facultad de Ingeniería,
Avenida Gran Bretaña 1111 Playa Ancha,
Valparaíso, Chile

H. Gomez (✉) · R. Henriquez · R. Schrebler
Instituto de Química, Facultad de Ciencias,
Pontificia Universidad Católica de Valparaíso,
Casilla 4059,
Valparaíso, Chile
e-mail: hgomez@ucv.cl

R. Marotti · E. Dalchiele
Departamento de Química y Bioquímica, Instituto de Física,
Facultad de Ingeniería,
Herrera y Reissig 565, C.C. 30,
11000 Montevideo, Uruguay

Introduction

High-quality one-dimensional nanostructures such as nanowires and nanorods are of great interest owing to their potential application in fields such as nanoscale electronics, optoelectronic devices, high-density magnetic memories, and electromechanical devices [1–7]. Particularly, ZnO is an important material for photonic and electrical applications due to its unique physical and chemical properties [8–11]. Fabrication of well-ordered nanowire arrays with good crystalline properties is a challenge toward the development of nano-optoelectronic devices [12]. Among different synthetic strategies, anodic oxide alumina template-assisted electrodeposition has been proven to be a useful method to obtain well-aligned, densely packed, and high aspect ratio ZnO nanowires in aqueous medium [13–18]. Nevertheless, $Zn(OH)_2$ is also formed competing with oxide formation [19], a non-desirable side effect for further technological applications. Non-aqueous solvent can be employed to address this issue, as is the case of dimethyl sulfoxide (DMSO) which has been successfully employed for the electrochemical growth of ZnO and CdO thin films [20, 21]. Hierarchical ZnO hexagonal nanorods prepared on fluorine-doped tin oxide glass substrates via electrodeposition from DMSO–H_2O solution has been recently reported [22]. Polycrystalline ZnO nanowires embedded in the pores of anodic alumina membrane (AAO) templates were electrodeposited by Wang

et al. [23] from a DMSO solution. They reported a wurtzite polycrystalline structure for the ZnO nanowires, stating that the different orientation growth is induced by defects in the wall of the template pores [18].

In the current work, we report on the preparation of ZnO nanowire arrays that grow preferentially oriented along the (0001) crystallographic direction from DMSO solutions containing zinc chloride and molecular oxygen as precursors. Except for the absence of KCl, the experimental conditions (applied potential and temperature) were similar to those employed in [23] where polycrystalline nanowires were obtained. To account for this different behavior, it is important to point out that the AAO template makes the electrochemical growth of zinc oxide complex because factors such as overpotential, temperature, zinc ion concentration, nature of the counter ion, etc., influence the local kinetics and, consequently, the nanowire growth mechanism. Given this complexity, any explanation regarding an actual growth mechanism within the AAO template must remain only speculative. Notwithstanding, considering that the nanowires were grown on a very thin layer of gold at the bottom of the template pores, as a first approximation, we have conducted chronoamperometric experiments in order to study the nucleation and growth mechanism of ZnO on a bulk gold electrode in a DMSO electrolytic solution. This approach allows understanding the role played by chloride ions in the initial steps of ZnO formation, which can be extended to its growth inside the template to account for the preferential crystallographic orientation observed in the corresponding X-ray diffraction (XRD) spectra.

Experimental

AAO membranes were prepared from a 99.99% aluminum foil (0.13-mm thickness, Sigma-Aldrich) by the two-step anodization technique as described in our previous paper [24, 25]. The grease on the aluminum surface was removed with detergent and then successively rinsed with acetone and water. The cleaned aluminum sheets were submitted to an annealing at 350 °C in air during 1 h using a Lindberg/Blue M model tube furnace. Next, the aluminum sheets were first etched with a 5% (*w*/*w*, weight percentage) NaOH solution and afterwards with diluted nitric acid 30% (volume percentage). Subsequently, the samples were mechanically polished with alumina (0.30- and 0.05-μm mesh), followed by 1 min of electropolishing at 15 V in a 40% H_2SO_4, 59% H_3PO_4, and 1% glycerin bath. After this treatment, the samples were submitted to a first anodization at 40 V during 6 h in a 0.3 M oxalic acid solution at 20 °C. The anodized layer was etched with a 5% H_3PO_4 and 1.8% $H_2Cr_2O_4$ solution at room temperature for 12 h. The ordered pore arrangement was achieved with a second anodization step that was performed under the same conditions as in the first one. A 0.10 M $CuCl_2$/20% HCl solution at room temperature was employed to remove the remaining aluminum from the alumina substrate. To remove the barrier layer and to open the pores at the bottom, the membrane was treated with 5% H_3PO_4 aqueous solution for 50 min and 5% NaOH aqueous solution for 5 min at room temperature. Subsequently, the pores were widened in a 0.085 M H_3PO_4 solution at 37 °C for 15 min. The formed membrane has a pore diameter of 40 nm and a thickness of 20 μm. The pore density was around 1.12×10^{10} pores cm^{-2} (estimated through SEM images) [15]. To facilitate the electric contact, a thin Au layer was sputtered on one side of the membrane.

The electrochemical cell consisted in a classical three-electrode setup. A Pt mesh and a $Ag/AgCl_{(sat.)}$ electrode (E= 0.194 V vs. SHE) were used as counter and reference electrodes, respectively. All the potentials in this work are referred to this reference electrode. The electrolyte was 0.05 M $ZnCl_2$ dissolved in DMSO (Merck). The electrodeposition was carried out a constant potential of −1.1 V with an Autolab (model PGSTAT 12) potentiostat. Temperature was kept at 85 °C, without solution stirring. Oxygen was bubbled until saturation into the electrolyte during the whole electrodeposition process.

Structural characterization of the ZnO nanowires embedded in alumina membranes was examined by XRD. The spectra were recorded with a Philips PW3710 diffractometer using Cu K_α radiation. The accelerating voltage was set at 40 kV with a 25-mA flux. Scatter and diffraction slits of 1 degree and 0.1-mm collection slit were used. The morphological characterization was carried out by SEM measurements with a JEOL 5900 LV apparatus.

Results and discussion

Electrodeposition of ZnO nanowires

According to previous studies [26, 27], the following mechanism accounts for the electrodeposition of ZnO in DMSO:

$$O_{2(sol)} + 1\bar{e} \rightarrow O^-_{2(sol)} \quad (1)$$

$$2O^-_{2(sol)} \rightarrow O_{2(sol)} + O^{2-}_{2(sol)} \quad (2)$$

$$O^{2-}_{2(sol)} + Zn^{(II)}_{(sol)} \rightarrow ZnO_{2(s)} \quad (3)$$

$$ZnO_{2(s)} \rightarrow ZnO_{(s)} + \frac{1}{2}O_{2(sol)} \quad (4)$$

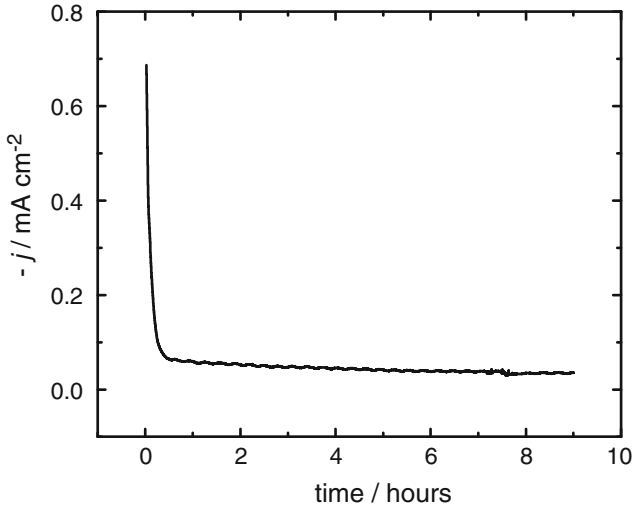

Fig. 1 Current–time response for the ZnO nanowire's electrodeposition from a 0.05 M $ZnCl_2$ DMSO solution saturated with oxygen at 85 °C. Electrodeposition potential, −1.1 V

ZnO formation occurs when the Zn(II) and O_2^{2-} ionic product at the interface reaches a critical value to start with ZnO_2 precipitation. As the analysis performed (*vide infra*) did not show evidences of ZnO_2 in the samples, it can be assumed that this compound was completely transformed into ZnO through step 4. Figure 1 shows the current vs. time transient obtained during the electrodeposition on the AAO membrane which differs from the typical curve for the nanowire's growth in porous templates [28–31]. This means that the electrodeposition took place to a point where the porous templates were not completely filled. Considering the amount of charge consumed in nanowire's formation (−1.71 C), the membrane thickness, the porous density, the ZnO molar mass and density, and the area exposed toward the solution (1.2 cm^2), the estimated nanowire's length is 7.75 μm (~39% of the pore's length), which agrees well with the evolution of the *j*/*t* transient depicted in the figure. The slowness of the electrodeposition process reveals that the diffusion of the electroactive species inside the pores is a determinant step for ZnO formation.

Morphological study of the ZnO nanowire arrays

Figure 2 shows SEM images of the ZnO nanowire arrays from two points of view. Figure 2a, b shows a surface view of free-standing ZnO nanowire arrays after an alkaline treatment with low magnifications, respectively, whereas Fig. 2c is a cross-sectional view of embedded ZnO nanowires into the anodic alumina membrane. Finally, Fig. 2d shows a high magnification view of free standing ZnO nanowires. From the SEM analysis of these free-standing ZnO nanowires, we could measure the ZnO nanowire diameter (approx. 36 nm) and the original pore diameter (approx. 40 nm). The little difference cannot be attributed to the shrinkage effect of ZnO but to a dissolution effect in alkaline media after a certain time of exposure to this media. Despite that, the measured diameter matches very well the alumina pore diameter, confirming the ability of alumina templates to prepare materials with sensitivity to pH changes or not. The length of the nanowires observed in the SEM images (~5.5 μm) is shorter than the theoretical length previously estimated (7.75 μm). This difference is attributed to the efficiency of the electrochemical process. In this case, the Faradaic efficiency is close to 71%, being

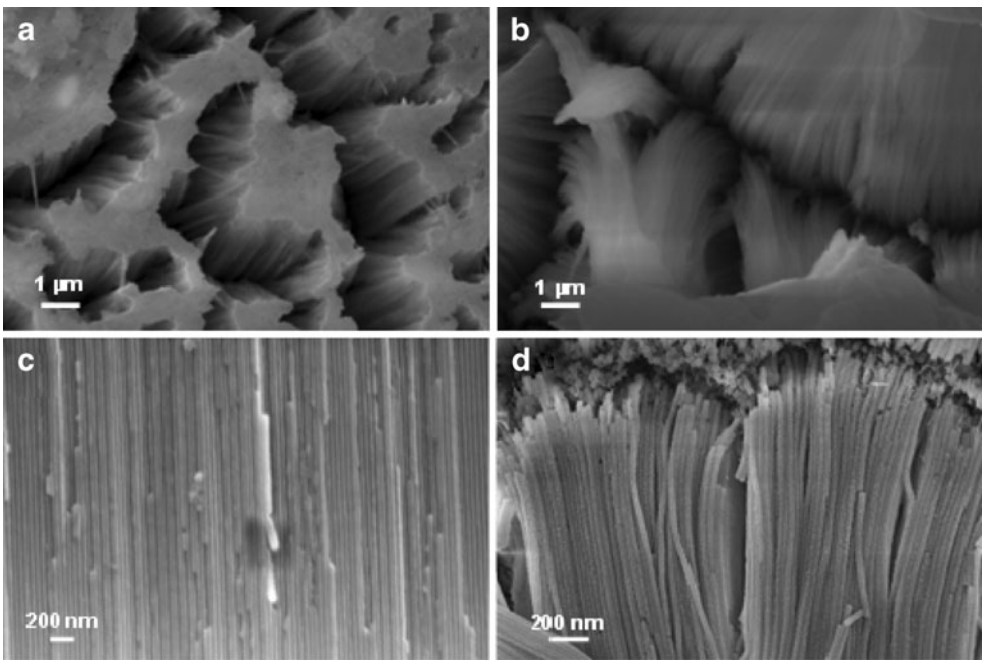

Fig. 2 SEM images of ZnO nanowires: **a**, **b** Top surface view of free standing ZnO nanowires with a low magnification. **c** Cross-sectional view of ZnO nanowires embedded into alumina template. **d** Lateral view of free-standing ZnO nanowires with a high magnification

the diffusion of electrogenerated oxygen species to the bulk solution the principal way to explain the loss of efficiency of the global process. According to this, the aspect ratio aspect (length-to-with ratio) of ZnO nanowires electrodeposited is 137.5.

Structural studies of the ZnO nanowire arrays

X-ray diffraction was employed to assess the phase structure and crystal orientation of the zinc oxide nanowire array alumina composites, anodic alumina membranes (AAM)/ZnO. Figure 3 shows a typical θ–2θ X-ray diffraction scan for ZnO nanowire arrays embedded in the alumina template that have been grown at −1.1 V, 85 °C; for comparison, its respective JCPDS pattern is also included [32]. The presence of only one diffraction peak corresponding to the (0002) plane of the ZnO wurzite structure can be appreciated, indicating an excellent preferential crystallographic orientation in the *c*-axis direction of these nanowire arrays over a large area (the Au diffraction peak due to the back side of the AAM template). Moreover, the last indicates a very high crystallinity of the grown ZnO nanowires. These results are aligned with those previously reported for the electrodeposition of ZnO nanorods without templates [33, 34] in which a preferred crystallographic orientation along the [0001] direction has been observed. However, Wang et al. [23] reported structural results of ZnO nanowires grown in an AAM template in a similar non-aqueous bath solution (DMSO) showing the presence of strong reflections corresponding to (1010), (0002), and (1011) planes wurtzite ZnO, indicating that ZnO nanowires were polycrystalline without obvious preferred crystallographic orientation.

In order to understand these different structural characteristics exhibited by the ZnO nanowires grown in very similar conditions, a more exhaustive analysis of both procedures has been done. In fact, in our case, the electrolytic bath is constituted by 0.05 M $ZnCl_2$, whereas the one employed by Wang et al. contained a higher total chloride concentration: 0.05 M $ZnCl_2$+0.1 M KCl. Then, a nucleation and growth mechanism study of the ZnO electrodeposition has been performed in order to understand the role of chloride anion influence, if any, on the nucleation and growth of ZnO and finally on the structural characteristics of the grown ZnO nanowires.

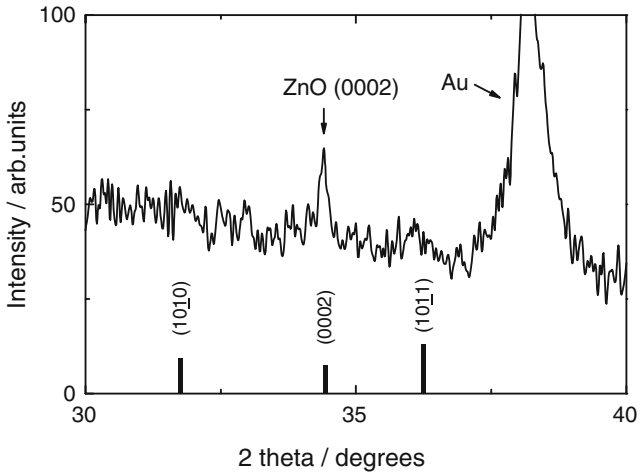

Fig. 3 X-ray diffraction pattern of the AAM/ZnO nanowire arrays electrochemically grown at −1.1 V, 85 °C. The corresponding line pattern of the bulk hexagonal of ZnO provided by the JCPDS database is also included

Nucleation and growth mechanism study

In order to study the nucleation and growth mechanism of ZnO electrodeposition and to investigate the influence of KCl addition, a chronoamperometric analysis (*j*/*t* transients) has been done. Chronoamperometric technique has just been used to describe the nucleation process during the initial few seconds of ZnO thin film electrodeposition [35]. Moreover, Tena-Zaera et al. [36] studied the role and the influence of chloride concentration on ZnO nanowire growth mechanism without template in aqueous media. They concluded that altering the Cl^- content in solution, the deposition rate and dimensions of ZnO single-crystal nanowire arrays are affected.

As was previously mentioned, a gold thin film has been sputtered onto the back side of the AAO template, and therefore, the pore bottom works as an Au nanoelectrode. In addition, as the template has parallel pore arrays with uniform diameters, the Au-coated AAO template can be considered as a porous nanoelectrode. However, in the present work, a massive macroscopic gold electrode has been chosen in order to carry out the mentioned chronoamperometric studies. This approach has been chosen in order to simplify the problem and with the idea to further extrapolate these results to the gold nanoelectrode/AAO system (within the limits that the different behavior of the macroelectrode compared with the nanoelectrode imposes) [37]. It is important to point out that the AAO template makes the growth mechanism of ZnO nanowires more complex [38]. In fact, it has also been shown that the electrochemical processes could be diffusion-limited within the porous electrode [39]. However, in spite of this difficulty, the nucleation and growth mechanism results in a gold macroelectrode which can be taken in a first approximation as the basis for understanding the nucleation and growth mechanism of the ZnO nanowires within the AAO template [37].

A set of current vs. time transients were obtained by the potential step method for a gold electrode in a similar electrolytic bath as that used for the ZnO nanowire growth (0.05 M $ZnCl_2$+saturated O_2 in DMSO) in the presence and in the absence of KCl. The steps were carried out starting

from a potential E_i=0 V, where no electrochemical process takes place to a deposition potential (E_d) in the range −1.0 V≥E_d≥−1.3 V, which is the zone where the ZnO electrodeposition process occurs. This potential range included both the main electrodeposition potential used in this work (E_d=−1.1 V) and that employed by Wang et al. [23] (E_d=−1.0 V). Figure 4 shows the experimental potentiostatic current density vs. time transients for ZnO electrodeposition onto a gold substrate at different applied potential values in the absence and presence of KCl. Differences in the shape of these transients can be attributed to the different nucleation and growth mechanisms that also should account for the different structural properties exhibited by the electrochemically grown ZnO nanowires. Moreover, the transients present the characteristic features

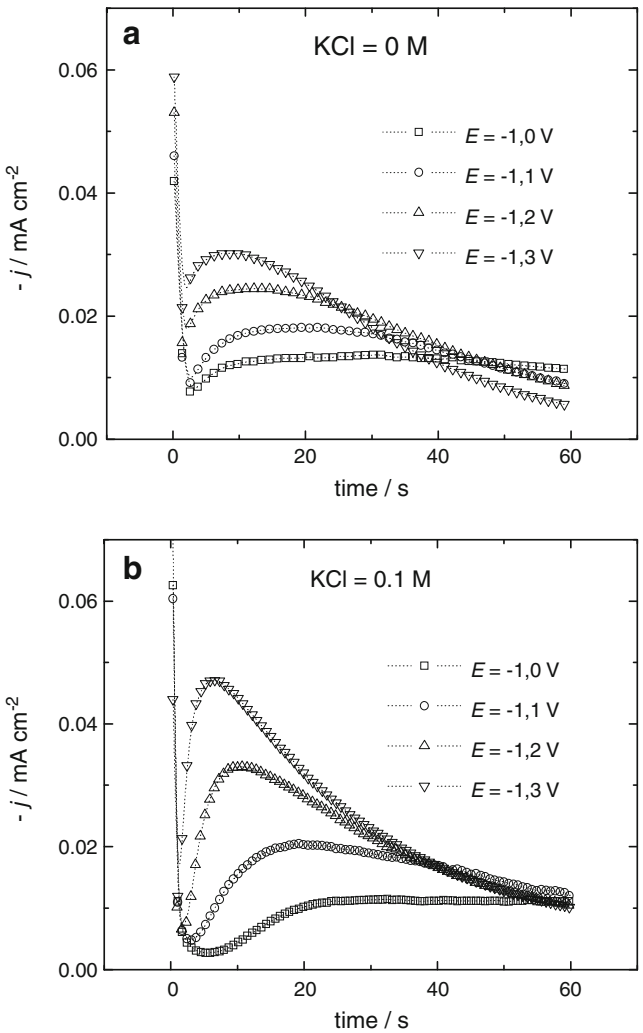

Fig. 4 Potentiostatic current density vs. time transients for the electrodeposition of ZnO onto a gold electrode at the potentials indicated from 0.05 M $ZnCl_2$+saturated O_2 in DMSO at 85 °C (experimental conditions employed in this work) (**a**); 0.05 M $ZnCl_2$+ 0.1 M KCl+saturated O_2 in DMSO at 85 °C (experimental conditions reported by Wang et al. [23]) (**b**)

of a nucleation process with three-dimensional growth of nuclei limited by the diffusion of the electroactive species. In both cases (in the absence and in the presence of KCl), a molecular oxygen concentration of approx. 2.45 mM in the DMSO-based solution has been considered [40, 41]. Consequently, the overall electrochemical process should be controlled by the molecular oxygen diffusion in solution. Then, the transient analysis was performed comparing the chronoamperometric curves with the adimensional theoretical curves for the diffusion-controlled nucleation and growth of crystals in three dimensions (3D), proposed by Scharifker and Hills [42]. The experimental transients are presented in a non-dimensional form by plotting $(j/j_m)^2$ vs. (t/t_m) and compared to the theoretical values obtained by plotting Eqs. 1 and 2 for instantaneous $(IN\text{-}3D)_{diff}$ and progressive $(PN\text{-}3D)_{diff}$ nucleation, respectively [42]:

Instantaneous nucleation

$$\left(\frac{j}{j_m}\right)^2 = \frac{1.9542}{t/t_m}\left\{1-\exp\left[-1.2564\left(\frac{t}{t_m}\right)\right]\right\}^2 \quad (1)$$

Progressive nucleation

$$\left(\frac{j}{j_m}\right)^2 = \frac{1.2254}{t/t_m}\left\{1-\exp\left[-2.3367\left(\frac{t}{t_m}\right)^2\right]\right\}^2 \quad (2)$$

where t_m and j_m are the coordinates of the time and current density maximum, and t and j are the time of the potential perturbation and recorded current density, respectively. Figure 5 shows the experimental data from Fig. 4 corresponding to the four applied potential values, presented in dimensionless form along with the theoretical dimensionless curves obtained from Eqs. 1 and 2. Without KCl in solution, the transients follow a $(IN\text{-}3D)_{diff}$ model, whereas in the presence of KCl, the transients follow a $(PN\text{-}3D)_{diff}$ model for all the applied potential steps in both cases.

Those different nucleation and growth mechanism behaviors observed without the addition of KCl in solution (instantaneous nucleation and growth mechanism) and with the presence of KCl in solution (progressive one) are in agreement with the XRD results for the ZnO nanowires. A limited number of nuclei can grow in an instantaneous nucleation process which is determined by the number of active site in the substrate. This deposition mode favors the growth of existing nuclei instead of the formation of new

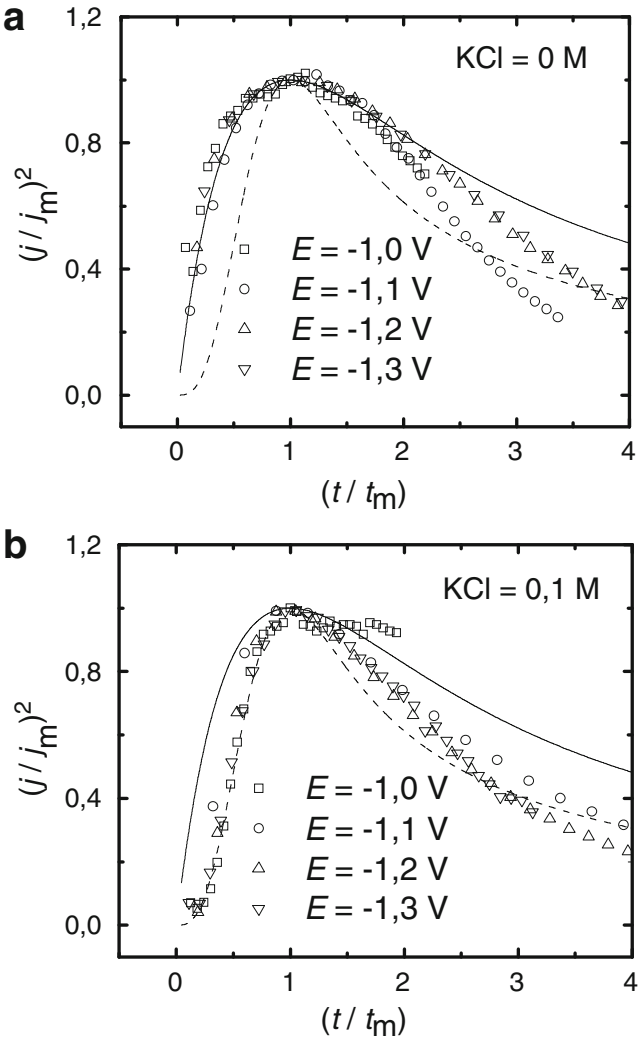

Fig. 5 Comparison of the theoretical non-dimensional plots for instantaneous $(IN\text{-}3D)_{diff}$ (*continuous line*) and progressive $(PN\text{-}3D)_{diff}$ (*dashed line*) nucleation and three-dimensional growth controlled by diffusion obtained using Eqs. 1 and 2, respectively, to the experimental current density transients in Fig. 4. *Symbols* represent the experimental data

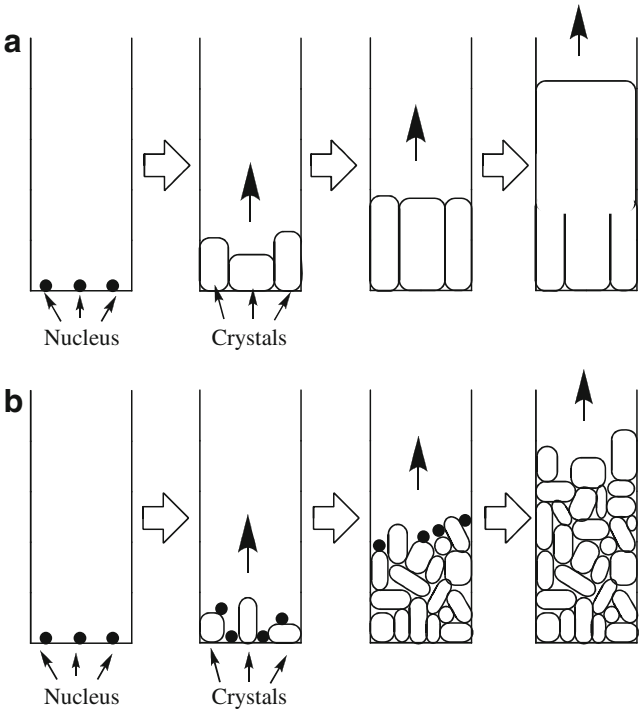

Fig. 6 Sketch of the nucleation and growth processes of ZnO nanowire grown by electrodeposition inside a pore. **a** Instantaneous nucleation (KCl=0 M). **b** Progressive nucleation (KCl=0.1 M)

ones, allowing to achieve a better crystalline quality and a preferentially orientated nanowire's growth, as is schematically shown in Fig. 6a. On the contrary, in a progressive nucleation growth mechanism, the number of nuclei increases as the electrodeposition time progresses. The latter should promote that the ZnO growth proceeds in a highly disordered way inside the template pores, arising in randomly oriented crystals (see Fig. 6b).

Conclusions

ZnO nanowire arrays were grown by potentiostatic cathodic electrodeposition on aluminum anodic oxide template (AAO) from DMSO solutions containing zinc chloride and molecular oxygen as precursors. The nanowires presented high aspect ratio and exhibited a very high crystallinity with a wurtzite crystal structure with preferential orientation along crystallographic *c*-axis. Chronoamperometric experiments performed on gold bulk electrodes in order to model this preferential growth revealed the influence of chloride ions in the oxide nucleation and growth mechanism. In the presence of KCl as supporting electrolyte, the *j*/*t* transients fitted a $(PN\text{-}3D)_{diff}$ model, whereas a $(IN\text{-}3D)_{diff}$ mechanism accounted for the nucleation and growth without KCl present in the solution. The $(IN\text{-}3D)_{diff}$ way of growing favors the growth of existing nuclei over the formation of new ones, allowing to achieve a better crystalline quality and a preferentially orientated ZnO growth. In a first approximation, these results give support to propose a simple model to understand the more complex growth process of the ZnO nanowires inside the pores of the AAO templates.

Acknowledgments This work was supported by FONDECYT (Chile) project 1080195 and DII, PUCV, project 037.108/2008. D. Ramirez thanks MECESUP UVA0604. EAD thanks PEDECIBA-Física and CSIC-UDELAR, Uruguay.

References

1. Cobden DH (2001) Molecular electronics—nanowires begin to shine. Nature 409(6816):32–33
2. Jie JS, Wang GZ, Han XH, Yu QX, Liao Y, Li GP, Hou JG (2004) Indium-doped zinc oxide nanobelts. Chem Phys Lett 387(4–6):466–470
3. Cui Y, Lieber CM (2001) Functional nanoscale electronic devices assembled using silicon nanowire building blocks. Science 291 (5505):851–853
4. Jie JS, Wang GZ, Han XH, Hou JG (2004) Synthesis and characterization of ZnO: in nanowires with superlattice structure. J Phys Chem B 108(44):17027–17031
5. Prinz GA (1998) Device physics—magnetoelectronics. Science 282(5394):1660–1663
6. Whitney TM, Jiang JS, Searson PC, Chien CL (1993) Fabrication and magnetic-properties of arrays of metallic nanowires. Science 261(5126):1316–1319
7. Li FY, Metzger RM, Doyle WD (1997) Influence of particle size on the magnetic viscosity and activation volume of alpha-Fe nanowires in alumite films. IEEE Trans Magn 33(5):3715–3717
8. Saito N, Haneda H, Sekiguchi T, Ohashi N, Sakaguchi I, Koumoto K (2002) Low-temperature fabrication of light-emitting zinc oxide micropatterns using self-assembled monolayers. Adv Mater 14 (6):418–421
9. Huang MH, Mao S, Feick H, Yan HQ, Wu YY, Kind H, Weber E, Russo R, Yang PD (2001) Room-temperature ultraviolet nanowire nanolasers. Science 292(5523):1897–1899
10. Lee JY, Choi YS, Kim JH, Park MO, Im S (2002) Optimizing *n*-ZnnO/*p*-Si heterojunctions for photodiode applications. Thin Solid Films 403:553–557
11. Liang S, Sheng H, Liu Y, Huo Z, Lu Y, Shen H (2001) ZnO Schottky ultraviolet photodetectors. J Cryst Growth 225(2–4):110–113
12. Liu CH, Zapien JA, Yao Y, Meng XM, Lee CS, Fan SS, Lifshitz Y, Lee ST (2003) High-density, ordered ultraviolet light-emitting ZnO nanowire arrays. Adv Mater 15(10):838–841
13. Li Y, Meng GW, Zhang LD, Phillipp F (2000) Ordered semiconductor ZnO nanowire arrays and their photoluminescence properties. Appl Phys Lett 76(15):2011–2013
14. Ramanathan S, Patibandla S, Bandyopadhyay S, Edwards JD, Anderson J (2006) Fluorescence and infrared spectroscopy of electrochemically self assembled ZnO nanowires: evidence of the quantum confined Stark effect. J Mater Sci Mater El 17(9):651–655
15. Ramirez D, Pauporte T, Gomez H, Lincot D (2008) Electrochemical growth of ZnO nanowires inside nanoporous alumina templates. A comparison with metallic Zn nanowires growth. Phys Status Solidi A 205(10):2371–2375
16. Wu MZ, Yao LZ, Cai WL, Jiang GW, Li XG, Yao Z (2004) Preparation and photoluminescence of ordered ZnO nanowire arrays. J Mater Sci Technol 20(1):11–13
17. Yuldashev SU, Choi SW, Kang TW, Nosova LA (2003) Growth of ZnO nanowires by electrochemical deposition into porous alumina on silicon substrates. J Korean Phys Soc 42:S216–S218
18. Zheng MJ, Zhang LD, Li GH, Shen WZ (2002) Fabrication and optical properties of large-scale uniform zinc oxide nanowire arrays by one-step electrochemical deposition technique. Chem Phys Lett 363(1–2):123–128
19. Peulon S, Lincot D (1998) Mechanistic study of cathodic electrodeposition of zinc oxide and zinc hydroxychloride films from oxygenated aqueous zinc chloride solutions. J Electrochem Soc 145(3):864–874
20. Gal D, Hodes G, Lincot D, Schock HW (2000) Electrochemical deposition of zinc oxide films from non-aqueous solution: a new buffer/window process for thin film solar cells. Thin Solid Films 361–362:79–83
21. Jayakrishnan R, Hodes G (2003) Non-aqueous electrodeposition of ZnO and CdO films. Thin Solid Films 440(1–2):19–25
22. Lu X-H, Wang D, Li G-R, Su C-Y, Kuang D-B, Tong Y-X (2009) Controllable electrochemical synthesis of hierarchical ZnO nanostructures on FTO glass. J Phys Chem C 113(31):13574–13582
23. Wang Q, Wang G, Xu B, Jie J, Han X, Li G, Li Q, Hou JG (2005) Non-aqueous cathodic electrodeposition of large-scale uniform ZnO nanowire arrays embedded in anodic alumina membrane. Mater Lett 59(11):1378–1382
24. Cortés A, Riveros G, Palma JL, Denardin JC, Marotti RE, Dalchiele EA, Gómez H (2009) Single-crystal growth of nickel nanowires: influence of deposition conditions on structural and magnetic properties. J Nanosci Nanotechnol 9:1992–2000
25. Green S, Badán JA, Gilles M, Cortes A, Riveros G, Ramírez D, Gómez H, Quagliata E, Dalchiele EA, Marotti RE (2007) Optical properties of nanoporous Al_2O_3 obtained by aluminium anodization. Phys Status Solidi C 4(2):618–621
26. Henriquez R, Froment M, Riveros G, Dalchiele EA, Gomez H, Grez P, Lincot D (2007) Electrodeposition of polyphasic films of zinc oxi sulfide from DMSO onto *n*-InP(100) and *n*-InP(111) single crystals in the presence of zinc salt, thiourea, and dissolved molecular oxygen. J Phys Chem C 111(16):6017–6023
27. Henriquez R, Gomez H, Grez P, Lincot D, Froment M, Dalchiele EA, Riveros G (2007) One-step electrodeposition of ZnO_2-ZnS thin-film mixtures onto *n*-InP(111) and *n*-InP(100) substrates. Electrochem Solid State Lett 10(11):D134–D138
28. Riveros G, Gomez H, Cortes A, Marotti RE, Dalchiele EA (2005) Crystallographically-oriented single-crystalline copper nanowire arrays electrochemically grown into nanoporous anodic alumina templates. Appl Phys A 81(1):17–24
29. Schonenberger C, vander Zande BMI, Fokkink LGJ, Henny M, Schmid C, Kruger M, Bachtold A, Huber R, Birk H, Staufer U (1997) Template synthesis of nanowires in porous polycarbonate membranes: electrochemistry and morphology. J Phys Chem B 101(28):5497–5505
30. Toimil-Molares ME, Buschmann V, Dobrev D, Neumann R, Scholz R, Schuchert IU, Vetter J (2001) Single-crystalline copper nanowires produced by electrochemical deposition in polymeric ion track membranes. Adv Mater 13(1):62–65
31. Valizadeh S, George JM, Leisner P, Hultman L (2002) Electrochemical synthesis of Ag/Co multilayered nanowires in porous polycarbonate membranes. Thin Solid Films 402(1–2):262–271
32. PD Joint Committee for Powder Diffraction Studies (JCPDS) File No. JCPDS 5-0664 (hexagonal wurtzite ZnO)
33. Elias J, Tena-Zaera R, Levy-Clement C (2008) Electrochemical deposition of ZnO nanowire arrays with tailored dimensions. J Electroanal Chem 621(2):171–177
34. Chen J, Ae L, Aichele C, Lux-Steiner MC (2008) High internal quantum efficiency ZnO nanorods prepared at low temperature. Appl Phys Lett 92(16):161906
35. Inamdar AI, Mujawar SH, Barman SR, Bhosale PN, Patil PS (2008) The effect of bath temperature on the electrodeposition of zinc oxide thin films via an acetate medium. Semicond Sci Technol 23(8):085013
36. Tena-Zaera R, Elias J, Wang G, Levy-Clement C (2007) Role of chloride ions on electrochemical deposition of ZnO nanowire Arrays from O-2 reduction. J Phys Chem C 111(45):16706–16711
37. Riveros G, Green S, Cortes A, Gomez H, Marotti RE, Dalchiele EA (2006) Silver nanowire arrays electrochemically grown into nanoporous anodic alumina templates. Nanotechnology 17 (2):561–570
38. Zhang XY, Zhang LD, Lei Y, Zhao LX, Mao YQ (2001) Fabrication and characterization of highly ordered Au nanowire arrays. J Mater Chem 11(6):1732–1734

39. Schuchert IU, Toimil-Molares ME, Dobrev D, Vetter J, Neumann R, Martin M (2003) Electrochemical copper deposition in etched ion track membranes—experimental results and a qualitative kinetic model. J Electrochem Soc 150(4):C189–C194
40. Arudi RL, Allen OA, Bielski HJB (1981) Some observations on the chemistry of KO_2—DMSO solutions. FEBS Lett 135(2):265–267
41. Fujinaga T, Izutsu K, Adachi T (1969) Polarographic studies of dissolved oxygen in DMSO–water mixtures. Bull Chem Soc Jpn 42:140–145
42. Scharifker B, Hills G (1983) Theoretical and experimental studies of multiple nucleation. Electrochim Acta 28(7):879–889